Wave propagation in beams with anti-symmetric piezoelectric shunting arrays*

Sheng-Bing Chen(陈圣兵)[1,†] and Gang Wang(王刚)[2]

[1] China Aerodynamics Research and Development Center, Mianyang 621000, China
[2] State Key Laboratory of Advanced Design and Manufacturing for Vehicle Body, Hunan University, Changsha 410082, China

(Received 12 July 2015; revised manuscript received 4 September 2015; published online 20 January 2016)

Piezoelectric shunting arrays are employed to control the wave propagation in flexible beams. Contrary to conventional symmetric configuration, a substrate beam with anti-symmetric shunting arrays is investigated by adapted transfer matrix method. Compared with symmetric scheme, the anti-symmetric one demonstrates some distinctive characteristics. Primarily, the longitudinal and flexural waves are coupled, so they are correlated and must be considered simultaneously. Moreover, the attenuation of flexural wave is much stronger in anti-symmetric scenario, while the longitudinal wave demonstrates the converse side. As a result, the anti-symmetric scheme can be utilized to improve the vibration isolation capability of shunting arrays. Finally, the theoretical analyses are validated by finite element simulations.

Keywords: piezoelectric shunting, metamaterial, phononic, band gaps

PACS: 43.20.Bi, 43.40.+s, 62.30.+d, 77.65.–j **DOI:** 10.1088/1674-1056/25/3/034301

1. Introduction

Elastic wave propagation in periodic structures has been researched for several decades.[1–3] The study of wave motion in periodic structures has been exerted primarily on pass band and stop band analyses. In recent years, the propagation of elastic waves in periodic composite materials, named phononic crystal (PCs), has received much attention.[4–10] The pioneering work of Liu *et al.* opened new fields of PCs.[6] They examined three-dimensional PCs consisting of cubic arrays of coated lead spheres immersed in an epoxy matrix, and proposed a new kind of gap formation mechanism, i.e., locally resonant (LR) band gap. More recently, the development of LR PCs has extended to newly emerging field: acoustic metamaterials.[11–13] Acoustic metamaterials are generally regarded as materials with artificial microstructures that possess unusual physical properties such as band gaps, negative refraction, acoustic cloaking, etc.

Structures periodically shunted by electrical resonant circuits can also produce locally resonant band gaps. Moreover, the band gaps can be tuned over desired frequency ranges conveniently through adjustment of the circuit parameters. Thorp *et al.* utilized an array of resonantly shunted piezoelectric patches mounted on a rod to create band gaps centered at the tuning frequencies of the shunting circuits.[14] Airold *et al.* proposed using multi-resonant shunts to form multiple band gaps in a beam.[15] Subsequently, they proposed to design one-dimensional tunable acoustic metamaterials through periodic arrays of resonant shunts.[16] The authors also did a lot of theoretical and experimental investigations on wave propagations in structures with shunting circuits,[17–21] and tried to utilized shunting arrays to isolate vibrations propagating in flexible structures. In all these studies, symmetric scheme is generally adopted, i.e., the piezoelectric patches are oppositely mounted on the top and bottom surfaces of the substrate structure. The resulting structure is symmetric with respect to the neutral surface, in which elongation and bending deformations are decoupled, so flexural and longitudinal waves are uncoupled. Consequently, asymmetric schemes lack of elaborate exploration, and some valuable properties need to be dug out.

In this paper, we propose an anti-symmetric scheme of shunting arrays instead of the conventional symmetric layout, and obtain the dispersion relation of coupled waves in the composite beam. The propagation constants are evaluated by transfer matrix method, which is adapted for anti-symmetric scenario. Compared with the symmetric scheme, the anti-symmetric configuration demonstrates some new properties. Specifically, the attenuation of flexural dominated wave in anti-symmetric layout is much stronger than that in symmetric one. However, the attenuation of longitudinal dominated wave shows the converse feature. Finally, the theoretical predications are verified by finite element simulations.

2. Structure configuration and mathematical models

The real structural configuration of the beam with antisymmetric piezoelectric shunting arrays is schematically shown in Fig. 1. Pairs of piezoelectric patches are periodically bonded to the surfaces of the substrate beam with infinite length, forming a superlattice structure. Each pair of piezo-

*Project supported by the National Natural Science Foundation of China (Grant No. 51322502).
†Corresponding author. E-mail: shengbingchen@cardc.cn
© 2016 Chinese Physical Society and IOP Publishing Ltd

patches is anti-symmetrically mounted on the top and bottom surfaces, respectively. Moreover, every piezo-patch is independently connected to a serial resistive-inductive (RL) shunting circuit with identical parameters.

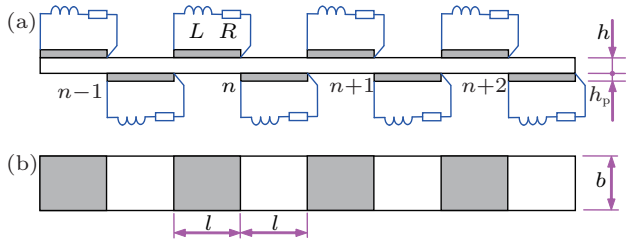


Fig. 1. (color online) Layout of the beam assembly. (a) Front view and (b) top view.

On the analogy of lattice dynamics, the wave motions in the above beam assembly can be derived from one single periodic element as shown in Fig. 2 (shunting circuits are omitted), combined with application of the Floquet theorem, i.e.,[22]

$$\begin{Bmatrix} u_{\mathrm{R}} \\ w_{\mathrm{R}} \\ w'_{\mathrm{R}} \end{Bmatrix} = \mathrm{e}^{\mu} \begin{Bmatrix} u_{\mathrm{L}} \\ w_{\mathrm{L}} \\ w'_{\mathrm{L}} \end{Bmatrix}, \tag{1}$$

$$\begin{Bmatrix} F_{\mathrm{R}} \\ M_{\mathrm{R}} \\ Q_{\mathrm{R}} \end{Bmatrix} = -\mathrm{e}^{\mu} \begin{Bmatrix} F_{\mathrm{L}} \\ M_{\mathrm{L}} \\ Q_{\mathrm{L}} \end{Bmatrix}, \tag{2}$$

where u and w are the longitudinal and flexural displacements, respectively. w' is the slope of flexural displacement, and the prime indicates the derivative. F, M, and Q are the resultant axial force, bending moment, and shear force on the beam cross-section, respectively. The suffixes L and R represent the left and right ends of the beam element. μ is propagation constant, which can be rewritten as

$$\mu = \delta + \mathrm{i}\varsigma, \tag{3}$$

in which δ and ς are called attenuation constant and phase constant, respectively. If the resulting δ is nil, the corresponding wave can propagate in the beam without decay; if the resulting δ is positive or negative, the corresponding wave will be enhanced or attenuated, respectively.

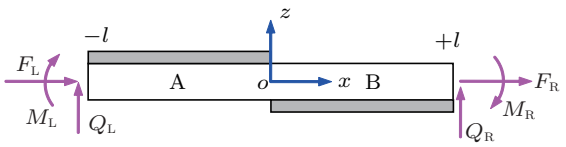


Fig. 2. (color online) Boundary forces acting on the beam element.

Both the beam segments A and B are asymmetrical with respect to the neutral surface of the substrate beam. As a result, the longitudinal and flexural motions in the segments are coupled. For simplicity, Euler–Bernoulli beam assumption is adopted. Consider an infinitesimally small element of segment A with length dx, as shown in Fig. 3. $F(x)$, $M(x)$, and $Q(x)$ are axial force, bending moment, and shear force on the cross-section, respectively. The deflection on the cross-section (ε) can be considered as the superposition of a pure elongation (ε_1) and a bending (ε_2) with respect to neutral surface of the substrate beam.

Hence, the strain on the cross-section can be written as

$$\varepsilon(x,z,t) = \frac{\partial u(x,t)}{\partial x} - z\frac{\partial^2 w(x,t)}{\partial x^2}, \tag{4}$$

where $u(x,t)$ and $w(x,t)$ are the longitudinal and flexural displacements, respectively.

Piezoelectric patches on the beam surfaces are polarized through z-axis, and assuming that all the surfaces are free of constraint except those along the x-axis. For simplicity, the directions along x, y, and z axes are represented by 1, 2, and 3 in the piezoelectric equations. Hence, the piezoelectric equations can be reduced to[14]

$$\begin{cases} S_1 = s_{11}^{\mathrm{E}} T_1 + d_{31} E_3, \\ D_3 = d_{31} T_1 + \varepsilon_{33}^{\mathrm{T}} E_3, \end{cases} \tag{5}$$

where S_1 and T_1 are mechanical strain and stress in the x-axis direction, respectively. s_{11}^{E} is compliance coefficient at constant electric field intensity. d_{31} is the piezoelectric constant that couples the mechanical and electrical properties. D_3 is the electric displacement on the electrodes. $\varepsilon_{33}^{\mathrm{T}}$ is the dielectric constant at constant stress, and E_3 is the electric field intensity in z-axis direction.

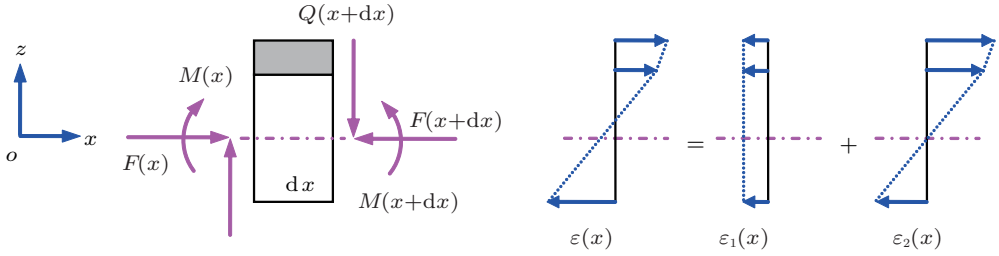


Fig. 3. (color online) Deformation in the cross-section of segment A.

Solving equation set (5) yields

$$D_3 = \frac{d_{31}}{s_{11}^{\mathrm{E}}} S_1 + \varepsilon_{33}^{\mathrm{S}} E_3, \tag{6}$$

where $\varepsilon_{33}^{\mathrm{S}}$ is the dielectric constant at constant strain, and can be written as

$$\varepsilon_{33}^{\mathrm{S}} = \varepsilon_{33}^{\mathrm{T}} - \frac{d_{31}^2}{s_{11}^{\mathrm{E}}}. \tag{7}$$

Each piezoelectric patch is attached to a serial RL shunting circuit as shown in Fig. 4. Hence, the electric current I_{s} can be given by

$$I_{\mathrm{s}} = -sQ_{\mathrm{s}} = \frac{V_{\mathrm{s}}}{R + Ls}, \tag{8}$$

where s is Laplace operator, Q_{s} and V_{s} are the quantities of electric charge and electric voltage on the electrodes, and V_{s} can also be written as

$$V_{\mathrm{s}} = E_3 h_{\mathrm{p}}. \tag{9}$$

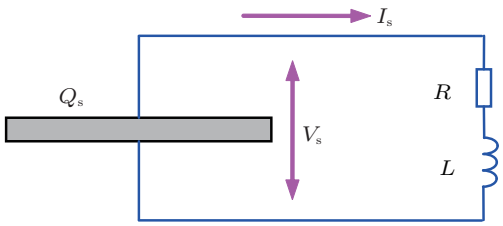


Fig. 4. (color online) Sketch map of the shunting circuit.

Substituting Eq. (9) into Eq. (8) yields

$$Q_{\mathrm{s}} = -\frac{E_3 h_{\mathrm{p}}}{s(R + Ls)}. \tag{10}$$

On the other hand, the amount of electrical charge on the electrode can also be given by

$$Q_{\mathrm{s}} = \iint_{A_{\mathrm{s}}} D_3 \mathrm{d}A, \tag{11}$$

where A_{s} is the area of the electrode, and $A_{\mathrm{s}} = bl$.

Substituting Eq. (6) into Eq. (11) yields

$$Q_{\mathrm{s}} = \frac{d_{31}}{s_{11}^{\mathrm{E}}} b \int_{-l}^{0} S_1 \mathrm{d}x + \varepsilon_{33}^{\mathrm{S}} E_3 A_{\mathrm{s}}. \tag{12}$$

Utilizing Eq. (4), the strain in the thin piezoelectric patches can be expressed as

$$S_1 = \varepsilon\left(x, \frac{h + h_{\mathrm{p}}}{2}, t\right) = \frac{\partial u(x,t)}{\partial x} - \frac{h + h_{\mathrm{p}}}{2} \frac{\partial^2 w(x,t)}{\partial x^2}. \tag{13}$$

Substituting Eq. (13) into Eq. (12), the integrating result is

$$Q_{\mathrm{s}} = \frac{d_{31}}{s_{11}^{\mathrm{E}}} b \left\{ [u(0,t) - u(-l,t)] - \frac{h + h_{\mathrm{p}}}{2} \left[\frac{\partial w(0,t)}{\partial x} - \frac{\partial w(-l,t)}{\partial x} \right] \right\} + \varepsilon_{33}^{\mathrm{S}} E_3 A_{\mathrm{s}}. \tag{14}$$

Combining Eqs. (10) and (14), the electric field intensity can be solved as

$$E_3 = -\frac{s(R + Ls) d_{31} b}{s_{11}^{\mathrm{E}} h_{\mathrm{p}} \left[1 + s(R + Ls) C_{\mathrm{p}}^{\mathrm{S}}\right]} \left\{ [u(0,t) - u(-l,t)] - \frac{h + h_{\mathrm{p}}}{2} \left[\frac{\partial w(0,t)}{\partial x} - \frac{\partial w(-l,t)}{\partial x} \right] \right\}, \tag{15}$$

where $C_{\mathrm{p}}^{\mathrm{S}}$ is the capacitance of the piezo-patch at constant strain, and

$$C_{\mathrm{p}}^{\mathrm{S}} = \frac{\varepsilon_{33}^{\mathrm{S}} A_{\mathrm{s}}}{h_{\mathrm{p}}}. \tag{16}$$

Substituting Eq. (15) into Eq. (5), the stress in the piezoelectric patch can be solved as

$$T_1 = \frac{1}{s_{11}^{\mathrm{E}}} S_1 + T_{\mathrm{a}}, \tag{17}$$

where

$$\begin{aligned} T_{\mathrm{a}} &= k_{\mathrm{s}} \left\{ [u(0,t) - u(-l,t)] - \frac{h + h_{\mathrm{p}}}{2} \left[\frac{\partial w(0,t)}{\partial x} - \frac{\partial w(-l,t)}{\partial x} \right] \right\}, \\ k_{\mathrm{s}} &= \frac{s(R + Ls) d_{31}^2 b}{\left(s_{11}^{\mathrm{E}}\right)^2 h_{\mathrm{p}} \left[1 + s(R + Ls) C_{\mathrm{p}}^{\mathrm{S}}\right]}. \end{aligned} \tag{18}$$

On the assumption of Euler–Bernoulli beam, the coupled longitudinal and flexural motions in the beam segment can be given by

$$\begin{aligned} &\Phi \frac{\partial^2 u(x,t)}{\partial x^2} - \Theta \frac{\partial^3 w(x,t)}{\partial x^3} - \Xi \frac{\partial^2 u(x,t)}{\partial t^2} + \Gamma \frac{\partial^3 w(x,t)}{\partial t^2 \partial x} = 0, \\ &\Psi \frac{\partial^4 w(x,t)}{\partial x^4} - \Theta \frac{\partial^3 u(x,t)}{\partial x^3} + \Xi \frac{\partial^2 w(x,t)}{\partial t^2} = 0, \end{aligned} \tag{19}$$

where $x \in (-l, 0)$ and

$$\begin{aligned} &\Phi = EA + E_{\mathrm{p}} A_{\mathrm{p}}, \quad \Theta = \frac{E_{\mathrm{p}} A_{\mathrm{p}} \left(h + h_{\mathrm{p}}\right)}{2}, \quad \Xi = \rho A + \rho_{\mathrm{p}} A_{\mathrm{p}}, \\ &\Gamma = \frac{\rho_{\mathrm{p}} A_{\mathrm{p}} \left(h + h_{\mathrm{p}}\right)}{2}, \quad \Psi = EI + E_{\mathrm{p}} I_{\mathrm{p}}. \end{aligned} \tag{20}$$

Here, E, A, ρ, I and E_{p}, A_{p}, ρ_{p}, I_{p} are Young's modulus, area of cross-section, density and moment of inertia of substrate beam and piezoelectric patch, respectively.

If harmonic motion at frequency ω is assumed, equation (19) can be reduced to

$$\begin{cases} \Phi \dfrac{\mathrm{d}^2 U(x)}{\mathrm{d}x^2} - \Theta \dfrac{\mathrm{d}^3 W(x)}{\mathrm{d}x^3} + \omega^2 \Xi U(x) - \omega^2 \Gamma \dfrac{\mathrm{d}W(x)}{\mathrm{d}x} = 0, \\ \Psi \dfrac{\mathrm{d}^4 W(x)}{\mathrm{d}x^4} - \Theta \dfrac{\mathrm{d}^3 U(x)}{\mathrm{d}x^3} - \omega^2 \Xi W(x) = 0, \end{cases} \tag{21}$$

where $U(x)$ and $W(x)$ are vibration amplitudes of longitudinal and flexural motions, respectively.

Applying Laplace transformation into Eq. (21) and eliminating $U(x)$ yield characteristic equation

$$a_0 s^6 + a_1 s^4 - a_2 s^2 - a_3 = 0, \tag{22}$$

where

$$a_0 = \frac{\Phi\Psi}{\Theta} - \Theta, \quad a_1 = \omega^2\left(\frac{\Xi\Psi}{\Theta} - \Gamma\right),$$
$$a_2 = \omega^2\frac{\Xi\Psi}{\Theta}, \quad a_3 = \omega^4\frac{\Xi^2}{\Theta}. \tag{23}$$

The solution of Eq. (21) can be written as

$$\begin{aligned} W(x) &= g_1\cos(\alpha x) + g_2\sin(\alpha x) + g_3\cos(\beta x) \\ &\quad + g_4\sin(\beta x) + g_5\cosh(\gamma x) + g_6\sinh(\gamma x), \end{aligned} \tag{24}$$

where g_i $(i = 1, 2, \ldots, 6)$ is undetermined coefficients. α, β, and γ are the solutions of Eq. (22), i.e.,

$$\alpha = \sqrt{2\sqrt{\frac{q}{3}}\cos\left(\frac{\pi+\varphi}{3}\right) + \frac{a_1}{3a_0}},$$
$$\beta = \sqrt{2\sqrt{\frac{q}{3}}\cos\left(\frac{\pi-\varphi}{3}\right) + \frac{a_1}{3a_0}},$$
$$\gamma = \sqrt{2\sqrt{\frac{q}{3}}\cos\left(\frac{\varphi}{3}\right) - \frac{a_1}{3a_0}}, \tag{25}$$

with

$$\begin{aligned} q &= \frac{a_2}{a_0} + \frac{1}{3}\left(\frac{a_1}{a_0}\right)^2, \\ \phi &= \cos^{-1}\left\{\left(\frac{27a_3}{a_0} - \frac{9a_1a_2}{a_0^2} - \frac{2a_1^3}{a_0^3}\right)\right. \\ &\quad \left.\Big/\left[2\left(\frac{a_1^2}{a_0^2} + \frac{3a_2}{a_0}\right)^{3/2}\right]\right\}. \end{aligned} \tag{26}$$

Substitution of Eq. (24) into Eq. (21) yields

$$\begin{aligned} U(x) &= g_1\zeta_1\sin(\alpha x) + g_2\zeta_2\cos(\alpha x) + g_3\zeta_3\sin(\beta x) \\ &\quad + g_4\zeta_4\cos(\beta x) + g_5\zeta_5\sinh(\gamma x) \\ &\quad + g_6\zeta_6\cosh(\gamma x), \end{aligned} \tag{27}$$

where

$$\zeta_1 = -\zeta_2 = -\frac{\alpha\Psi - \alpha^{-3}\omega^2\Xi}{\Theta},$$
$$\zeta_3 = -\zeta_4 = -\frac{\beta\Psi - \beta^{-3}\omega^2\Xi}{\Theta},$$
$$\zeta_5 = -\zeta_6 = -\frac{\gamma\Psi - \gamma^{-3}\omega^2\Xi}{\Theta}. \tag{28}$$

On the other hand, the axial force $F(x)$, bending moment $M(x)$, and shear force $Q(x)$ can be given by

$$F(x) = \Phi\frac{\mathrm{d}U(x)}{\mathrm{d}x} - \Theta\frac{\mathrm{d}^2W(x)}{\mathrm{d}x^2} + T_aA_p,$$
$$M(x) = \Psi\frac{\mathrm{d}^2W(x)}{\mathrm{d}x^2} - \Theta\frac{\mathrm{d}U(x)}{\mathrm{d}x} + \frac{h+h_p}{2}T_aA_p,$$
$$Q(x) = \Psi\frac{\mathrm{d}^3W(x)}{\mathrm{d}x^3} - \Theta\frac{\mathrm{d}^2U(x)}{\mathrm{d}x^2}. \tag{29}$$

Hence, the vector

$$\boldsymbol{Z}_1(x) = \left[\, U(x)\ F(x)\ W(x)\ W'(x)\ M(x)\ Q(x) \,\right]^{\mathrm{T}}$$

can be expressed as

$$\boldsymbol{Z}_1(x) = \boldsymbol{T}_1(x)\boldsymbol{g}, \tag{30}$$

where $\boldsymbol{T}_1(x)$ can be derived by substituting Eqs. (24) and (27) into equation set (29), $\boldsymbol{g}$ is the vector of undetermined coefficients and $\boldsymbol{g} = \{g_i\}^{\mathrm{T}}$, $i = 1, 2, \ldots, 6$.

By analogy, the counterpart vector $\boldsymbol{Z}_2(x)$ in segment B can also be derived from the aforementioned procedures, and given by

$$\boldsymbol{Z}_2(x) = \boldsymbol{T}_2(x)\boldsymbol{h}, \tag{31}$$

where $\boldsymbol{h}$ is the vector of undetermined coefficients in segment B.

The continuity between the segment A and B in the n-th periodic element can be expressed as

$$\begin{cases} \boldsymbol{Z}_{n,1}(0) = \boldsymbol{Z}_{n,2}(0), \\ \boldsymbol{Z}_{n+1,1}(-l) = \boldsymbol{Z}_{n,2}(l), \end{cases} \tag{32}$$

where the subscripts n and $n+1$ represent the n-th and $(n+1)$-th periods, respectively.

Therefore,

$$\boldsymbol{g}_{n+1} = \boldsymbol{T}\boldsymbol{g}_n, \tag{33}$$

where $\boldsymbol{T}$ is the transfer matrix of the beam element, and

$$\boldsymbol{T} = \boldsymbol{T}_1^{-1}(-l)\boldsymbol{T}_2(l)\boldsymbol{T}_2^{-1}(0)\boldsymbol{T}_1(0). \tag{34}$$

On the other hand, utilizing Eqs. (1) and (2), we have

$$\boldsymbol{g}_{n+1} = \mathrm{e}^{\mu}\boldsymbol{g}_n. \tag{35}$$

Substituting Eq. (35) into Eq. (34) yields

$$(\boldsymbol{T} - \mathrm{e}^{\mu})\boldsymbol{g}_n = 0. \tag{36}$$

Consequently, the propagation constant μ can be obtained by solving the eigenvalue of transfer matrix $\boldsymbol{T}$.

3. Result and discussion

In the numerical calculation, epoxy (Young's modulus $E = 4.35 \times 10^9$ Pa, Poission's ratio $\upsilon = 0.37$, and density $\rho = 1180$ kg/m^3) and PZT-5H (compliance coefficient $s_{11}^{\mathrm{E}} = 16.5 \times 10^{-12}$ m^2/N, piezoelectric constant $d_{31} = -2.74 \times 10^{-10}$ C/N, dielectric constant $\varepsilon_{33}^{\mathrm{T}} = 3.01 \times 10^{-8}$ F/m, and density $\rho_{\mathrm{p}} = 7500$ kg/m^3) are selected as the materials of substrate beam and piezoelectric patches, respectively. The geometrical parameters are as follows: $l = 0.03$ m, $b = 0.02$ m,

$h = 0.005$ m, and $h_p = 0.0002$ m. The shunting circuit parameters are selected at $R = 200\ \Omega$ and $L = 0.6$ H. Employing the foregoing transfer matrix method, the propagation constants of the beam with anti-symmetric piezoelectric shunting arrays are examined.

Figure 5 shows the propagation constant of waves propagating in the beam with the prescribed parameters. There are two types of coupled waves propagating in the beam. The first type is quasi-longitudinal wave mode (QLM), whose dispersion is weak. The other one is quasi-flexural wave mode (QFM), of which the dispersion with frequency is quite strong. Both the two wave modes show an attenuation region (called band gap), of which the locations are quite close. Notice, however, that the band-gap extent and attenuation magnitude of QFM are much larger than those of the QLM. As a result, the decay of QFM by shunting arrays are much more efficient.

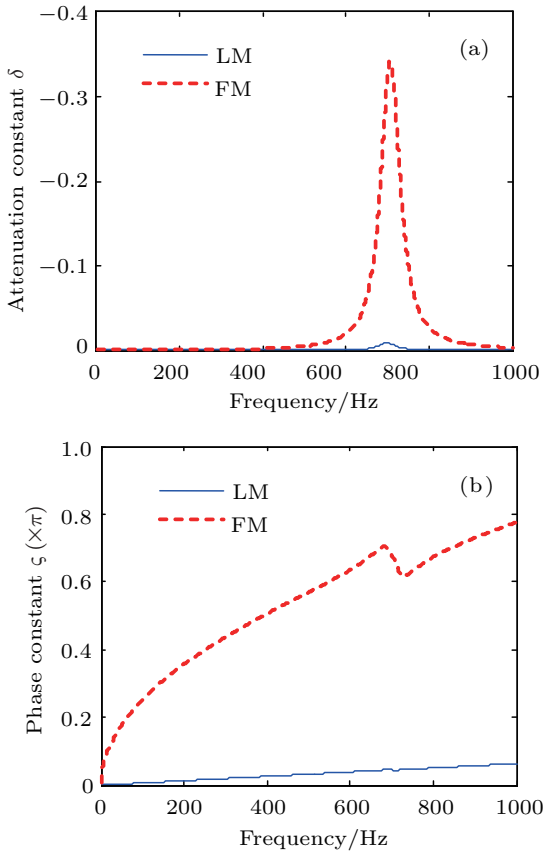


Fig. 5. (color online) (a) Attenuation constant and (b) phase constant of the wave motions.

As the considered wave motions are coupled, it is of interest to draw a comparison with uncoupled ones. The conventional configuration, which is generally symmetric, also bears two types of wave motions, *viz.* flexural wave and longitudinal wave. However, these two waves propagate independently in the beam. The comparison of attenuation constant between coupled and uncoupled wave motions are illustrated in Fig. 6. In Fig. 6(a), one can find that the attenuation of uncoupled (symmetric) longitudinal wave in the band gaps is much larger than that of coupled (anti-symmetric) longitudinal wave. In contrast, the attenuation of uncoupled (symmetric) flexural wave in the band gap is much smaller than that of coupled (anti-symmetric) flexural wave, as shown in Fig. 6(b). As a result, the attenuation of flexural wave is enhanced by substituting anti-symmetric configuration for the convention symmetric one. This anti-symmetric configuration can be utilized to suppress flexural wave propagation in beams much more efficiently. As piezoelectric patches are mounted on the surfaces of the substrate beam, more mechanical energy will be concentrated in the patches when the beam subjected to bending deformation. As a result, more mechanical energy can be transformed and coupled in the shunting circuits, resulting in more efficient attenuation of the flexural wave.

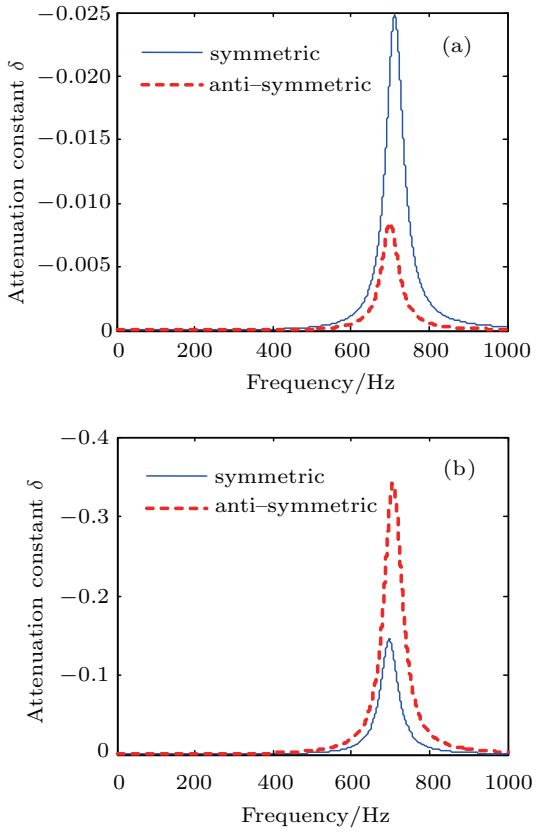


Fig. 6. (color online) Comparison between symmetric and anti-symmetric configuration. Propagation constant of longitudinal wave (a) and flexural wave (b).

In order to verify the above theoretical analyses, two finite element models with anti-symmetric and symmetric shunting arrays, consisting of 12 periods, are built in COMSOL, respectively. When longitudinal excitation is applied on the left end of the beam, the transmission properties of longitudinal (symmetric) and quasi-longitudinal (anti-symmetric) waves propagating in the beam are demonstrated in Fig. 7(a). In order to characterize the band gap location, the transmission property

of the longitudinal wave in the beam without internal resonance ($L = 0$ H) is also plotted in the diagram. Comparing the three curves, it is observed that a transmission dip is generated when the piezoelectric patches are shunted by resonant circuits. However, the shunting arrays with symmetric configuration show a stronger attenuation in the transmission dip. This result is in accordance with the theoretical analysis in Fig. 6(a). The transmission properties of flexural (symmetric) and flexural dominated (anti-symmetric) waves are presented in Fig. 7(b), when the left end of the beam is exerted on a transverse excitation. Comparing the different curves, one can find that resonant shunting circuits induce a transmission dip in the flexural wave as well. Contrary to the longitudinal wave, the shunting arrays with anti-symmetric configuration demonstrate much stronger attenuation ability in the band gap, which agree well with the theoretical predication in Fig. 6(b). In a word, the finite element simulations validate the theoretical predications, and prove correctness of the adapted transfer matrix derivation.

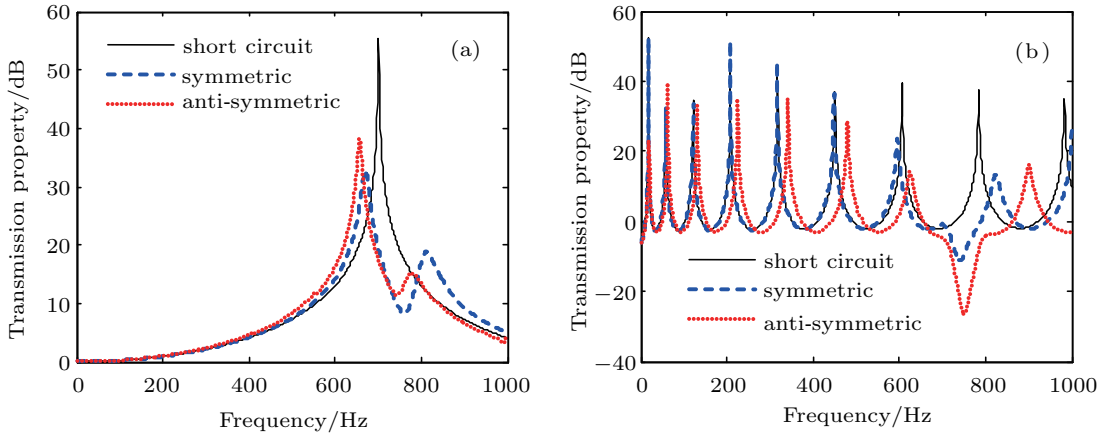


Fig. 7. (color online) Longitudinal (a) and flexural (b) wave transmission properties of the beam.

4. Conclusions

Wave propagation and attenuation in beams with anti-symmetric piezoelectric shunting arrays are investigated in this paper. Transfer matrix method is adapted for characterizing wave motions in the anti-symmetric model. In contrast to symmetric scenario, the longitudinal and flexural waves are coupled in anti-symmetric situation. As a result, some distinctive features are observed. First of all, the vibration energy is transformed between longitudinal and transverse degrees of freedom. Second, the attenuation of flexural wave is much stronger if the anti-symmetric configuration is adopted, which can be utilized to enhance vibration isolation capability of shunting arrays. Finally, the theoretical predications are verified by finite element simulations in COMSOL.

References

[1] Mead D J 1970 *J. Sound Vib.* **11** 181
[2] Mead D J 1986 *J. Sound Vib.* **104** 9
[3] Mead D J and Markus S 1983 *J. Sound Vib.* **90** 1
[4] Kushwaha M S, Halevi P, Dobrzynski L and Djafari-Rouhani B 1993 *Phys. Rev. Lett.* **71** 2022
[5] Sigalas M 1998 *J. Appl. Phys.* **84** 3026
[6] Liu Z, Zhang X, Mao Y, Zhu Y Y, Yang Z, Chan C T and Sheng P 2000 *Science* **289** 1734
[7] Wang G, Wen X, Wen J, Shao L and Liu Y 2004 *Phys. Rev. Lett.* **93** 154302
[8] Wen J H, Yu D L, Xiao Y and Wen X S 2009 *Chin. Phys. B* **18** 2404
[9] Chen A L, Tong L and Wang Y S 2015 *Chin. Phys. B* **24** 066101
[10] Huang P P, Yao Y W, Wu F G, Zhang X, Li J and Hu A Z 2015 *Chin. Phys. B* **24** 054301
[11] Li J and Chan C T 2004 *Phys. Rev. E* **70** 055602
[12] Fang N, Xi D, Xu J, Ambati M, Strituravanich W, Sun C and Zhang X 2006 *Nat. Mater.* **5** 452
[13] Milton G W 2007 *New J. Phys.* **9** 359
[14] Thorp O, Ruzzene M and Baz A 2001 *Smart Mater. Struct.* **10** 979
[15] Airoldi L and Ruzzene M 2011 *J. Intell. Mater. Syst. Struct.* **10** 979
[16] Airoldi L and Ruzzene M 2011 *New J. Phys.* **13** 113010
[17] Chen S, Wen J, Wang G, Yu D and Wen X 2012 *J. Intell. Mater. Syst. Struct.* **23** 1613
[18] Chen S, Wang G, Wen J and Wen X 2013 *J. Sound Vib.* **332** 1520
[19] Wang G, Chen S and Wen J 2011 *Smart Mater. Struct.* **20** 015026
[20] Chen S B, Wen J H, Yu D L, Wang G and Wen X S 2011 *Chin. Phys. B* **20** 014301
[21] Chen S B, Wen J H, Wang G, Han X Y and Wen J H 2011 *Chin. Phys. Lett.* **28** 094301
[22] Farzbod F and Leamy M J 2009 *J. Sound Vib.* **325** 545